

# Generation and evaluation of physically inspired synthetic mammograms

Predrag Bakic<sup>a,b</sup>, Michael Albert<sup>b</sup>, Dragana Brzakovic<sup>a</sup>, and Andrew D.A. Maidment<sup>b</sup>

**Abstract** – A software breast phantom, based upon a breast tissue model derived from physical properties of breast anatomy, has been developed for mammography simulation. Synthetic mammograms, obtained by applying a breast compression model and an x-ray acquisition model to the software breast phantom, were compared by quantitative and qualitative means with real mammograms at different scales. Good agreement was observed for two texture measures at a resolution of 500  $\mu\text{m}/\text{pixel}$ .

**Key words** – mammography, tissue model, texture analysis.

## I. INTRODUCTION

Recently, we proposed a method for performing a mammography simulation that relates the 3-D arrangement of adipose and fibroglandular tissue with the mammographic appearance of the breast<sup>1</sup>. The main purpose of such a simulation is to improve our understanding of mammograms including the effects of breast positioning and compression. Our simulation consists of a breast tissue model (a software breast phantom), a breast compression model, and an x-ray acquisition model.

The aim of our mammography simulation is not to model a particular patient but to include characteristic breast structures, distributed in a realistic fashion. The software breast phantom therefore consists of regions with varying mixtures of adipose and fibroglandular tissue. Breast compression during the exam is approximated by a deformation model and the elastic properties of breast tissue. Synthetic mammograms are obtained by simulating the x-ray image acquisition of the compressed software breast phantom.

Physical phantoms have been developed in breast imaging for a variety of reasons, including quality control and optimization of mammographic systems. Such phantoms have taken a number of forms from simple geometric models to complex tissue simulating objects. The ACR mammographic accreditation phantom consists of a uniform block of PMMA with embedded structures of varying contrast and size corresponding to fibers, specks, and masses. Phantoms such as this, however, provide only a rudimentary resemblance to the breast. They lack overlapping anatomic structures that form a characteristic parenchymal pattern or texture in mammograms. Breast phantoms made of preserved tissue specimens offer realistic mammographic appearance, but are less durable and cannot be fabricated in multiple identical copies. An anthropomorphic breast phantom<sup>2</sup> was designed to overcome these limitations by milling a block of plastic according to the pixel densities of a digitized mammogram. However, it is difficult to manufacture many different anthropomorphic phantoms due to the cost of fabrication.

The proposed software breast phantom and the anthropomorphic phantom have a common approach of relating realistic tissue distribution to mammographic appearance. In addition to being robust and reproducible, the software phantom offers an additional advantage of flexibility. A set of synthetic mammograms with different simulated properties of breast tissue or different acquisition parameters can be easily obtained without repeated exposure of patient volunteers or redesigning and fabricating physical phantoms.

Synthetic mammogram generation has been reported in the literature previously. One recently reported method<sup>3</sup> applied a sophisticated mathematical approach based upon the random field approximation and self-similar filtering. This method was successful in matching statistical characteristics of real mammograms, but there is no easily discernable relationship between physical properties of breast tissue and the algorithms used. In a separate mammography simulation<sup>4</sup>, similar to our own, a software breast phantom was developed. However, this work lacked a breast compression model, and the modeled anatomic structures of the breast were simpler, concentrating primarily on breast ducts.

Synthetic mammograms obtained by our mammography simulation were evaluated by comparing them to real mammograms. Quantitative properties of the mammographic texture were used for comparison. This paper presents results of this texture analysis.

## II. SOFTWARE BREAST PHANTOM

The software breast phantom is divided into two regions - one composed predominantly of adipose tissue, and one composed predominantly of fibroglandular tissue. Each tissue type has a number of associated physical properties including elasticity modulus and x-ray attenuation coefficient. The boundary between the adipose and the fibroglandular regions follows the one illustrated in many textbooks (e.g., Kopans<sup>5</sup>, Lamarque<sup>6</sup>) and is approximated by an ellipsoidal shape. The internal structure of the regions is modeled using their description in histologic slices and anatomic textbooks<sup>6</sup>. Cooper's ligaments and the fatty compartments within the adipose breast region are modeled by shells of fibroglandular tissue. The fatty compartments within the fibroglandular region are modeled by discrete regions of adipose tissue. The shape of the compartments is currently approximated by spheres. The ductal network is modeled by a computer generated ramified tree<sup>7</sup> using parameters inferred from galactography images.

<sup>a</sup>Department of Electrical Engineering and Computer Science, Lehigh Univ., Bethlehem, PA 18015; prb3@lehigh.edu

<sup>b</sup>Department of Radiology, Thomas Jefferson Univ., Philadelphia, PA 19107

A breast phantom is illustrated in Figure 1. Further details of the software breast phantom construction have been published previously<sup>1</sup>.

A model of breast compression was developed to estimate deformation of the software breast phantom. Deformations of breast slices (normal to the compression plates) are analyzed separately. Each slice is approximated as a 2-D composite beam. Beam components have elastic properties of adipose and fibroglandular tissue as found in the literature<sup>8</sup>. Deformed slices are stacked to produce a model of the compressed breast. Deformation of the internal structure of the adipose and fibroglandular tissue regions transforms the spherical adipose compartments into ellipsoids.

Synthetic mammograms are obtained using the synthetically compressed software breast phantom and a model of x-ray acquisition. The acquisition model accounts for the x-ray attenuation coefficients of the adipose and fibroglandular tissue, the projective nature of the x-ray acquisition, and the relationship between x-ray energy received and film density<sup>9</sup>. Figure 2 shows a synthetic mammogram obtained using this technique.

### III. EVALUATION OF SYNTHETIC MAMMOGRAMS

We evaluated the mammography simulation by comparison with real mammograms using quantitative and qualitative measures of texture. Digitized mammograms of normal cases from the MIAS and Lehigh University databases were used for this comparison. The synthetic images were generated at a resolution of 250  $\mu\text{m}$ , which is comparable to that of the databases. Parameters controlling the distribution of the breast tissue (e.g., the distribution of Cooper's ligaments within adipose tissue, and fatty cavities within fibroglandular tissue) in the model were adjusted to match the statistical properties of the data. Laws texture energy measures and fractal analysis were used to characterize the real and synthetic mammograms. Texture analysis was performed at two resolutions: 250  $\mu\text{m}$  and 500  $\mu\text{m}$  (the latter obtained by averaging 2x2 pixel blocks). Subimages of size 25 mm x 25 mm were selected from real and synthetic mammograms. Separate comparisons were made for subimages containing predominantly adipose tissue and predominantly fibroglandular tissue.

Laws texture energy is computed by taking the ratio of two measures capturing different texture properties (e.g., edges, waves, ripples, etc.). The R5R5 mask was convolved with image data from selected regions. The convolved data were averaged on a 15x15 window and normalized by the L5L5 feature mask. This method produces a measure that is related to local roughness of mammogram texture and has been used before in mammogram analysis<sup>10</sup>. Texture energy histograms were then computed.

Several fractal analysis methods have been published<sup>11-13</sup> for mammography. We have chosen the blanket method<sup>12</sup>. Fractal dimension describes self-similarity properties of an image at different scales. For the purposes of this discussion, consider image intensities in a mammogram as the height of a surface. In the case of a fractal surface the value of the surface area decreases with increasing unit measure (i.e., increasing the scale variable  $\epsilon$ ). The gradient on a  $\log A_\epsilon - \log \epsilon$  plot is

related to fractal dimension as  $\log A_\epsilon = \log K + (2-D) \log \epsilon$ , where  $A_\epsilon$  is the surface area at the scale  $\epsilon$ , and  $D$  is the fractal dimension. The scale variable  $\epsilon$  is incremented at every step of the blanket algorithm, allowing one to compute the fractal dimension from the  $\log A_\epsilon - \log \epsilon$  plot. Values of such a local fractal dimension were averaged within a 15x15 window around each pixel, producing the fractal descriptors used for texture analysis. Histograms of these averaged values of fractal dimensions were compared between real and synthetic tissue subimages. Parameters for the fractal analysis were selected to correspond to the parameters of texture energy analysis. Moreover, similar values of parameters were suggested as optimal in the literature<sup>12</sup>.

An additional analysis of sensitivity of the fitted values of the fractal dimension to the range of scale values  $\epsilon$  used in the blanket algorithm was performed, since there have been questions regarding the accuracy of the blanket method when computed at coarser scales<sup>13</sup>. Fractal dimension was computed at every step of the algorithm as the linear regression of the function  $\log A_\epsilon - \log \epsilon$  through three neighboring points. The obtained values of the scale dependent fractal dimension were averaged over 15x15 neighborhoods.

To quantify the comparison of two histograms, we use the correlation coefficient defined as  $\sum_i (f_i g_i) / (\sum_i f_i^2 \sum_i g_i^2)^{1/2}$  where summation runs over histogram bins.

An experienced mammographer and three medical physicists performed a subjective comparison of the simulated and real mammographic subregions. The comparison was made on the basis of both mammographic texture and perceived realism of the simulated structures.

### IV. RESULTS AND DISCUSSION

Laws texture energy histograms are shown in Figure 3 for real and synthetic mammograms at a resolution of 500  $\mu\text{m}$ . The Laws feature values for the synthetic mammograms are in the range of 0.02-0.05 for fibroglandular regions and in the range of 0.025-0.10 for adipose regions. These data closely agree with the range of feature values computed from subimages of real mammograms. Moreover, the distribution of the features values is similar for each region type (correlation  $\approx 70\%$  for the adipose and  $\approx 90\%$  for the fibroglandular tissue). Values of the same feature computed at a resolution of 250  $\mu\text{m}$  show less agreement (i.e., less overlap of the histograms for synthetic and real mammograms: correlation  $\approx 60\%$  for the adipose and  $\approx 10\%$  for the fibroglandular tissue).

Values of the fractal dimension at the resolution of 500  $\mu\text{m}$ , for both the adipose and fibroglandular tissue regions, are in the range of 2.2-2.8 when computed on the real mammograms and in the range of 2.2-2.6 for the synthetic mammograms. Better agreement between the real and synthetic mammograms was observed for the adipose tissue (correlation  $\approx 80\%$  for adipose vs.  $\approx 30\%$  for fibroglandular). At the resolution of 250  $\mu\text{m}$ , values of the fractal dimension are in the range of 2.1-2.7 for both real and synthetic mammograms and both tissue types, showing better agreement between the real and simulated fibroglandular regions than at the 500  $\mu\text{m}$  resolution (correlation  $\approx 90\%$  for adipose and  $\approx 80\%$  for fibroglandular).

When analyzing sensitivity of the fractal dimension to the range of scales used for linear regression, two scale ranges were used:  $\varepsilon=1,3$ ; yielding the fractal dimension denoted as  $D_{1,3}$  and  $\varepsilon=2,4$  used to calculate the fractal dimension  $D_{2,4}$ . In the case of the real mammograms it was observed at both resolutions of 250  $\mu\text{m}$  and 500  $\mu\text{m}$  that  $D_{1,3} \leq D_{2,4}$  for the subimages with predominantly fibroglandular tissue; the values for the adipose tissue showed the inverse trend, i.e.,  $D_{1,3} \geq D_{2,4}$ . The fractal dimensions computed on the synthetic mammograms for both types of tissue followed the observed trend to a lesser degree, (i.e., the overlap of the histograms for the  $D_{1,3}$  and  $D_{2,4}$  was larger..) especially at the resolution of 250  $\mu\text{m}$ , resulting in poorer agreement of the synthetic and real data. The histograms of  $D_{1,3}$  and  $D_{2,4}$  are shown in Figure 4, for adipose (upper graph) and fibroglandular tissue (lower graph).

In the subjective texture comparison a mammographer and three medical physicists perceived little difference between the real and synthetic subregions when viewing from 2 to 3 times the usual distance for mammogram analysis. When examined closely, differences appear. Namely, the synthetic pattern corresponding to an adipose region lacks the organization of blood vessels, and the simulated ellipsoidal fatty compartments have notably artificial appearance. Better agreement was perceived when comparing the real and synthetic fibroglandular regions. In addition, it was noticed that the border between the adipose and fibroglandular phantom regions appeared as a very clear geometrically regular separation between the bright and the dark part on a synthetic mammogram degrading the subjective perception of the whole image. We modified our model by adding a small random variation (less than 5%) when calculating the border between the compressed adipose and fibroglandular phantom regions. This has greatly improved the realistic visual appearance of the whole synthetic mammogram.

Comparing the obtained results for both the Laws texture energy descriptor and the fractal dimensions, better agreement between the real and synthetic mammograms was observed at the resolution of 500  $\mu\text{m}$  than at the resolution of 250  $\mu\text{m}$ . Similarly, better subjective visual appearance of synthetic mammograms was perceived when doubling the viewing distance (which corresponds to reducing the image resolution by half). A reason for this is the fact that our breast simulation approach is based on the large and middle scale anatomic structures (e.g., two tissue regions, Cooper's ligaments, fatty cavities, and ductal network). Improving details of the simulation at the small scales requires more knowledge about the microscopic 3-D properties of breast tissue and their relation with the mammographic appearance.

#### V. CONCLUSIONS

Starting from an understanding of the macroscopic anatomic tissue organization we were able to design a software breast phantom. Applying our previously developed mammography simulation to the breast phantom, we have generated synthetic mammograms. Qualitatively, the visual appearance of the generated images is similar to real mammograms, but the geometrically regular features present

in the simulations are visible upon close inspection. Quantitatively, the synthetic mammograms exhibit similar ranges of values for several texture features. Discrepancies between the synthetic and real images are more evident for texture measures that emphasize smaller spatial scales, in agreement with the qualitative visual assessment. Extensions of our model might simulate the variable anatomic structure sufficiently well to be used in the development of CAD (computer-aided diagnosis) algorithms that attempt to detect lesions in the presence of the background structured noise<sup>14</sup>. Extensions might include 3-D models of abnormalities based on their spatial analysis, e.g., a model of microcalcifications based on multiple view studies<sup>15</sup>.

The use of computed phantoms such as described here could be more appropriate than fabricating physical phantoms for certain applications, particularly when interest in anatomical variability necessitates the use of a large image database. The parameters in our model are traceable to the underlying anatomical structure. Thus, our approach is complementary to purely statistical approaches<sup>3</sup>.

#### REFERENCES

1. P. Bakic and D. Brzakovic, "Simulation of digital mammogram acquisition," SPIE Medical Imaging, 3659: 866-873, (eds.) J.M. Boone and J.T. Dobbins III, San Diego, CA, 1999
2. C.B. Caldwell and M.J. Yaffe, "Development of an Anthropomorphic Breast Phantom," Med. Phys., 17 (2): 273-280, 1990.
3. J.J. Heine, S.R. Deans, R.P. Velthuisen, and L.P. Clarke, "On the Statistical nature of Mammograms," Med. Phys., 26 (11): 2254-2265, 1999.
4. P. Taylor, R. Owens, and D. Ingram, "Simulated Mammography Using Synthetic 3D Breasts," in Digital Mammography Nijmegen, 1998, (eds.) N. Karssemeijer et al., 283-290, Kluwer, Dordrecht, The Netherlands, 1998.
5. D. Kopans, Breast Imaging, Lippincott-Raven, Philadelphia, PA, 1998.
6. J.L. Lamarque, The Breast Clinical Radiodiagnosis: An Atlas and Text, Wolfe Medical Publications, London, UK, 1981.
7. X.G. Viennot, G. Eyrolles, N. Janey, and D. Arques, "Combinatorial Analysis of Ramified Patterns and Computer Imagery of Trees," Computer Graphics, 23 (3): 31-40, 1989.
8. A. Sarvazyan et al., "Biophysical Bases of Elasticity Imaging," in Acoustic Imaging, 21: 223-240, (ed.) J.P. Jones, 1995.
9. R.P. Highnam, J.M. Brady, and B.J. Shephstone, "Computing the Scatter Component of Mammographic Images," IEEE Trans. Med. Imag., 13 (2): 301-313, 1994.
10. P. Miller and S. Astley, "Automatic Detection of Breast Asymmetry Using Anatomical Features," in State of the Art in Digital Mammographic Image Analysis, (eds.) K.W. Bowyer and S. Astley, 247-261, World Scientific, Singapore, 1994.
11. C.B. Caldwell, S.J. Stapleton, D.W. Holdsworth, R.A. Jong, W.J. Weiser, G. Cooke, and M.J. Yaffe, "Characterization of Mammographic Parenchymal Pattern by Fractal Dimension," Phys. Med. Biol., 35 (2): 235-247, 1990.
12. Lefevbre, H. Benali, R. Gilles, E. Kahn, and R. Di Paola, "A Fractal Approach to the Segmentation of Microcalcifications in Digital Mammograms" Med. Phys., 22 (4): 381-390, 1995.
13. A.I. Penn and M.H. Loew, "Estimating Fractal Dimension with Fractal Interpolation Function Models," IEEE Trans. Med. Imag., 16 (6): 930-937, Dec. 1997.
14. F.O. Buchod, C.K. Abbey, and M.P. Eckstein, "Further investigation of the effect of phase-spectrum on visual detection in structured backgrounds," SPIE Medical Imaging, 3663: 273-281, (ed.) E.A. Krupinsky, San Diego, CA, 1999.
15. A.D.A. Maidment, M. Albert, E.F. Conant, and S.A. Feig, C.W. Piccoli, and M. Albert, "Three-dimensional Analysis of Breast Calcifications," in Digital Mammography (eds.) K. Doi et al., 245-250, Excerpta Medica ICS-1119, Elsevier Scientific, The Netherlands, 1996.

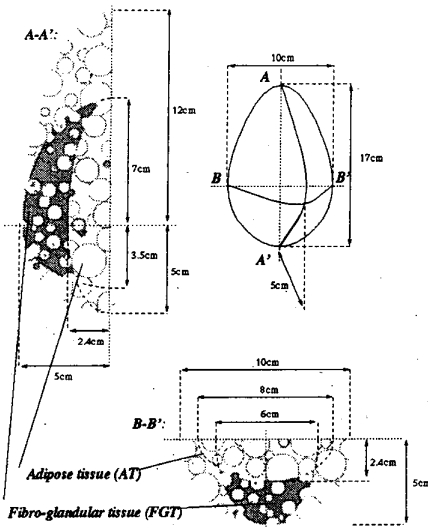
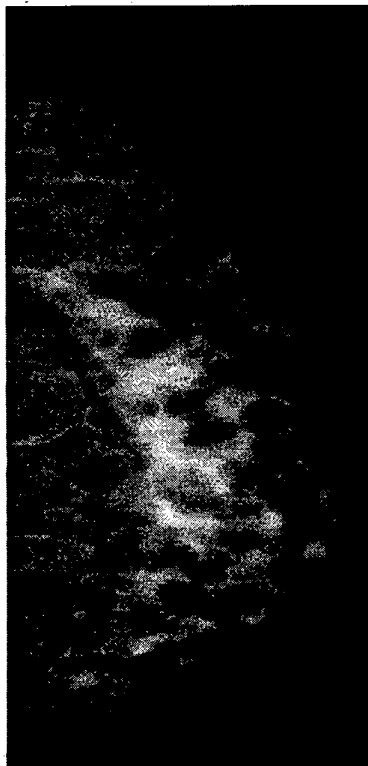


Figure 1: Sections of the software breast phantom, showing borders and internal structure of the regions with predominantly adipose and fibroglandular tissue.

Figure 2: A synthetic mammogram generated by simulation using the breast phantom. Image is produced assuming 20 keV and 5 cm overall thickness.



Real & Synth Mammo RR Histograms at 500um resol.

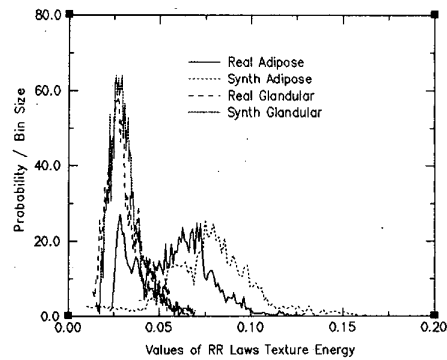
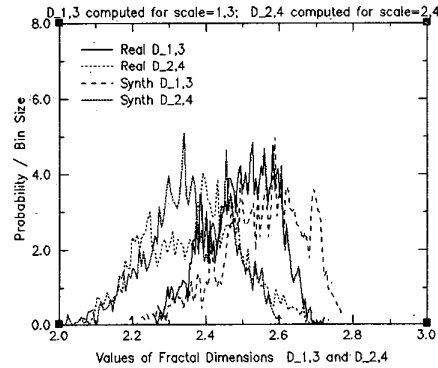


Figure 3: Histograms of Laws RR feature computed on 25 mm x 25 mm samples from the real and synthetic, predominantly adipose or fibroglandular tissue, at 500 μm.

Real & Synth Adipose FD Histograms at 500um resol.



Real & Synth Glandular FD Histograms at 500um resol.

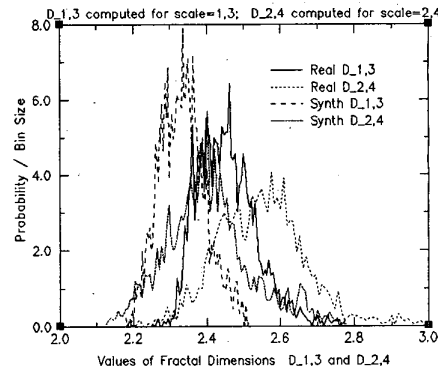


Figure 4: Histograms of fractal dimensions, for two different scale ranges (1-3 and 2-4), on adipose (upper graph) and fibroglandular (lower graph) tissue samples